# Dual-spectrum laser source based on fiber continuum generation for integrated optical coherence and multiphoton microscopy

**Benedikt W. Graf**
**Zhi Jiang**
**Haohua Tu**
**Stephen A. Boppart**
University of Illinois at Urbana-Champaign
Beckman Institute for Advanced Science and Technology
Department of Electrical and Computer Engineering
Biophotonics Imaging Laboratory
405 North Mathews Avenue
Urbana, Illinois 61801

**Abstract.** A single-laser dual-spectrum source designed for integrated optical coherence and multiphoton microscopy is demonstrated. The source implements the laser characteristics needed to optimally perform both modalities while extending the spectral range for this imaging technique. It consists of a widely tunable, mode-locked, Ti-sapphire laser with a portion of its output spectrally broadened via continuum generation in a photonic crystal fiber. The continuum-broadened beam allows for enhanced optical sectioning with optical coherence microscopy, while the unbroadened beam from the ultrashort-pulse Ti-sapphire laser optimally excites fluorescent markers. The noise power of the continuum-broadened beam is less than 1.1 dBm/Hz higher than the Ti-sapphire laser in the range from 1 Hz to 25 MHz, and the fiber shows no sign of damage after ~100 h of use. We demonstrate the use of this source across a wide spectral range by imaging green fluorescent protein-transfected mouse fibroblast cells costained with fluorescent dyes that are maximally excited at various wavelengths. Images of unstained *in vivo* human skin are also presented. This source extends the feasibility of this integrated imaging modality and will facilitate new investigations in *in vivo* microscopy, tissue engineering, and cell biology. © *2009 Society of Photo-Optical Instrumentation Engineers.* [DOI: 10.1117/1.3147422]

Keywords: multimodality imaging; optical coherence microscopy; multiphoton microscopy; continuum generation.

Paper 08406RR received Nov. 14, 2008; revised manuscript received Mar. 27, 2009; accepted for publication Mar. 31, 2009; published online Jun. 4, 2009.

## 1 Introduction

Integrated optical coherence (OCM) and multiphoton microscopy (MPM) is a technique that allows structural and functional properties of biological tissue to be imaged simultaneously. OCM combines the coherence gating of OCT with a high numerical aperture to provide high-resolution, scattering-based images with deeper penetration in scattering media than reflectance confocal microscopy.[1] MPM, which is based on two-photon excited fluorescence or harmonic generation, provides high-resolution images of specific functional molecules or regions of a sample. MPM typically has at least a twofold improvement in penetration depth over fluorescence confocal microscopy.[2] Penetration depth in tissue for both OCM and MPM is superior because these modalities operate in the near-infrared wavelength range where there is less scattering and absorption than in the visible range. The integration of these two imaging techniques is attractive for investigations in *in vivo* microscopy, tissue engineering, and cell and tumor biology. Endogenous or exogenous functional markers can be visualized with MPM in the context of their surrounding microstructural environment as visualized with OCM. The deep

penetration depth offered by both techniques extends the ability to assess different characteristics of thick, highly scattered tissue or tissue models at cellular-level resolution. Understanding cell dynamics in three-dimensional environments is a goal of cell biology with important clinical and research applications. Studies have used OCM/MPM to monitor wound healing in skin-equivalent tissue models[3] and to perform optical biopsies of thick tissue samples.[4] It has also been used to examine the structural origins of scattering contrast in individual cells.[5]

Although OCM and MPM can be performed simultaneously with a single laser source, each imaging modality demands different characteristics from the source to perform optimally. For MPM, ultrafast lasers such as Ti-sapphire lasers are the most efficient means of exciting two photon events. Investigations have found that MPM efficiency is proportional to the inverse of the laser pulse duration.[6] However, when considering transform limited pulses, the pulse duration is also inversely proportional to the spectral bandwidth. As most fluorophores have a limited wavelength range where efficient two-photon excitation occurs, the advantages of using ultrashort pulses can be negated by inefficient absorption across the broad bandwidth. As a result of this tradeoff, tun-

Address all correspondence to: Stephen A. Boppart, M.D., Ph.D., Beckman Institute for Advanced Science and Technology, 405 N. Mathews Avenue, Urbana, IL 61801; Tel: 217-244-7479; Fax: 217-333-5833; E-mail: boppart@illinois.edu.

able Ti-sapphire lasers with pulses in the range of ∼100 fs and thus, relatively narrow bandwidths (∼10 nm) are typically used for MPM. For OCM, a broad spectrum is desired because the coherence length is inversely dependent on the source bandwidth. Although axial OCM resolution is often determined by the confocal parameter of a high-numerical-aperture objective, high detection sensitivity and high contrast rejection of out-of-focus light is dependent on the coherence length.[1] Thus, broad bandwidth is needed to optimize optical sectioning capability. A tunable spectrum is also desired for OCM as it enables spectroscopic OCM (SOCM) analysis over a broad wavelength range. SOCM is an extension of OCM that provides additional contrast in biological specimens based on the spectrum of the backscattered light.[7,8]

Past studies utilizing integrated OCM/MPM used a single, fixed center wavelength, broadband Ti-sapphire laser.[9–11] For reasons stated, a tunable source with both a narrowband and a broadband portion would provide better performance and optimization for both imaging modalities. A recent study combined a broadband laser and a separate tunable Ti-sapphire laser for simultaneous MPM and phase-sensitive OCM.[12] We demonstrate in this paper a novel single-laser, dual-spectrum source for use in an integrated-spectral-domain OCM and MPM microscope. This source is implemented by spectrally-broadening a portion of a widely-tunable Ti-sapphire laser by continuum generation in a photonic crystal fiber. The source output is a beam consisting of the original spectrum (for MPM) and a continuum broadened spectrum (for OCM). Continuum generation in commercially available conventional single-mode fibers has been used as a simple and cost-effective way to create a broad spectrum source for OCT.[13] However, degradation of the optical spectrum, output power, and physical properties of the fiber is common and problematic for stable use as an optical source.[14] Continuum generation has also been demonstrated in highly nonlinear photonic crystal fibers[15] and tapered large-mode photonic crystal fibers.[16] The fiber chosen for this source is an endlessly single-mode photonic crystal fiber. This fiber is both cost-effective and capable of sufficient and stable spectral broadening for use in OCM over roughly a 300 nm tuning range.

The tunable, dual-spectrum source extends the optical sectioning capability of OCM while allowing a wide range of fluorescent markers to be targeted. The ability to acquire OCM and MPM images with this source over a wide wavelength range is demonstrated by imaging fluorescently labeled mouse fibroblast cells at three different wavelengths. Because deep penetration in tissue is ultimately the key advantage of integrated OCM/MPM over confocal microscopy, images of unlabeled *in vivo* human skin are taken at different depths. The optimized performance of both modalities enabled by this source extends the feasibility of OCM/MPM for investigations in *in vivo* microscopy, tissue engineering, and cell biology.

## 2 Single-Laser, Dual-Spectrum Source for Integrated OCM and MPM

Figure 1 shows the schematic of the dual-spectrum laser source (region I) within the integrated OCM/MPM system (region II). The laser is a high-power, widely tunable Ti-sapphire laser (Mai-Tai HP, Spectra-Physics). The linearly po-
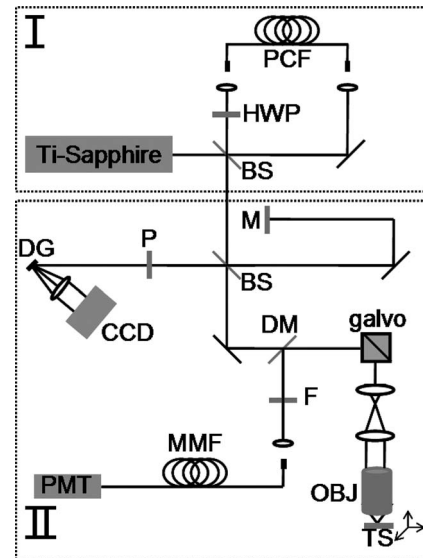


**Fig. 1** Schematic of the dual spectrum source (region I) and the integrated OCM/MPM microscope (region II). Abbreviations: BS, beam splitter; DG, diffraction grating; DM, dichroic mirror; F, emission filter; HWP, half-wave plate; M, mirror; MMF, multimode fiber; OBJ, objective lens; P, polarizer; PCF, photonic crystal fiber; PMT, photomultiplier tube; TS, translation stage.

larized output from this laser is divided by a 90/10 beamsplitter into two beams. The higher power beam is coupled by a 0.4 NA aspheric lens into an ∼2-m-long photonic crystal fiber with a numerical aperture (NA) of 0.1 and a mode field diameter of 6 $\mu$m (LMA-8, Crystal Fibre A/S). The spectrally broadened OCM beam is collimated, and the linear polarization is rotated 90 deg by an achromatic half-waveplate before being recombined with the narrowband beam at the original beamsplitter. The linear polarization of the OCM beam after continuum generation is sufficiently maintained, enabling orthogonal polarization between the narrowband MPM beam and the broadband OCM beam. This allows the MPM beam to be blocked by a polarizer when acquiring the spectral interference pattern for OCM detection. The wavelength of the laser is controlled via a personal computer. Tuning the wavelength requires adjustment of the spectrometer diffraction grating and a simple alignment of the input fiber to maximize power coupling. The output of the dual-spectrum source is subsequently used for imaging.

The experimental setup of the integrated microscope has been previously described in detail[9] but is summarized here. In the OCM/MPM system the beam is split into the reference and sample arms of the interferometer. In the sample arm the beam is expanded by a telescope and focused by a microscope objective (20X, 0.95 NA, water immersion, Olympus, Inc.) onto the sample. The sample is positioned on a motorized stage which is scanned to acquire the images. Alternatively, a pair of galvanometers positioned before the telescope can scan the beam across the sample. The epi-collected MPM fluorescent signal is diverted by a long-pass dichroic mirror and bandpass filtered. This filter is easily interchanged to detect various fluorescence or second-harmonic generation signals. The fluorescence signal is detected by a photomultiplier tube. At the output of the interferometer the polarizer (LP-
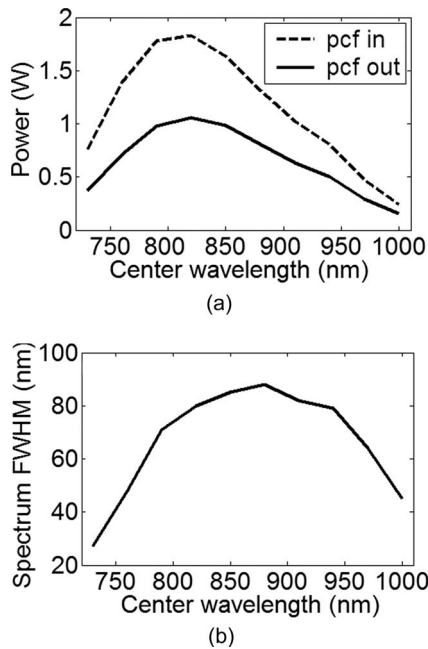
**Fig. 2** Wavelength-dependent characteristics of continuum generation in the dual-spectrum source. Plot (a) shows the input (dashed line) and output (solid line) power of the photonic crystal fiber. The fiber output is the available power for OCM. Plot (b) shows the spectral bandwidth of the broadened beam. The bandwidth of the pump laser is 5–10 nm, depending on wavelength.



**Fig. 3** Ti-sapphire pump spectra (dotted lines) and corresponding broadened spectra (solid lines) at (a) 750, (b) 850, and (c) 920 nm center wavelengths. The insets show the combined spectra incident on the sample.

NIR050, Thorlabs) blocks the MPM portion of the spectrum. At 800 nm the polarizer provides ~30 dB attenuation of the MPM beam and ~2 dB attenuation of the OCM beam. The spectral interference pattern of the reference and sample arm beams is detected for OCM acquisition by a spectrometer based on a diffraction grating and CCD line camera (P2-22-02k40, Dalsa). The frame rate for the line camera depends on the speed and mode of image acquisition (galvanometer or stage) and ranges from 5–35 kHz. Processing the OCM images included compensating for unbalanced dispersion in the sample arm and for nonuniform distribution of the spectrum on the CCD due to nonlinearity of the diffraction grating. A computer synchronizes the scanning of the beam or the stage movement and the acquisition and processing of MPM and OCM data.

The power of the MPM and OCM source can be independently controlled by a set of neutral density filters. Figure 2 shows input and output power of the photonic crystal fiber as well as the spectral broadening across the tuning range of the laser. The majority of the laser output is used for continuum generation because the degree of spectral broadening is dependent on the input power. The power of the narrowband MPM reflected from the beam splitter ranges from 30 to 300 mW in the wavelength range 730–1000 nm. There are additional losses in the OCM/MPM microscope due to the beamsplitter and objective. The splitting of power between the OCM and MPM beams could be directly controlled by using a polarization-dependent beam splitter and a half-waveplate instead of a 90/10 beamsplitter.

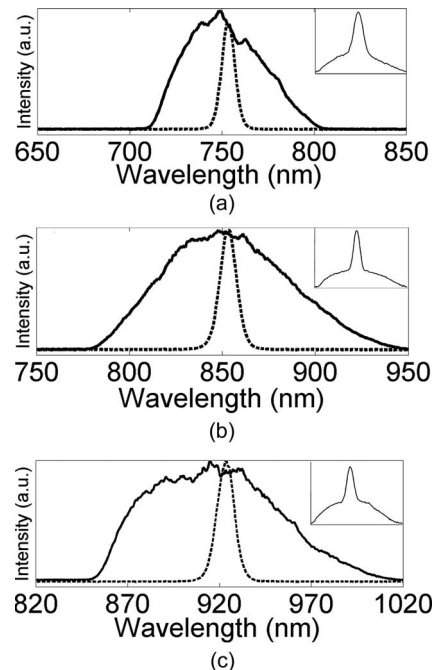The pump spectrum and broadened spectrum at three different wavelengths are shown in Fig. 3. These three wavelengths were chosen because they correspond to efficient two-photon absorption wavelengths for the three different fluorescent markers used in imaging the fibroblast cells. The insets in Fig. 3 show the combined spectra used for imaging. The FWHM of the broadened spectra at 750, 850, and 920 nm is 52, 86, and 82 nm, respectively. Because the coherence length is proportional to the square of the center wavelength and inversely proportional to the bandwidth, it is roughly equivalent at these three wavelengths despite differences in the generated bandwidth. The corresponding calculated FWHM coherence lengths in air at each of these center wavelengths are 4.7, 3.7, and 4.6 $\mu$m, respectively. This represents a coherence length 5–8 times shorter than that of the pump laser alone, allowing greater rejection of out-of-focus light and thus, greater sensitivity and optical sectioning capability.

Crucial to using this source for OCM imaging is the stability of the continuum generation. Degradation of the spectral broadening due to light-induced structural modification is common for Ge-doped conventional fibers.[17] Amplitude fluctuations of the spectrum caused by noisy nonlinear processes limit the feasibility of using continuum generation in highly nonlinear photonic crystal fibers as an optical source for OCT or OCM. Our source utilizes a pure silica photonic crystal fiber and is stable because these fibers lack the Ge-related photosensitive impurities that cause fiber degradation. This fiber has shown no sign of degradation after ~100 h of use. In addition, this fiber is operated in the normal dispersion regime (the zero-dispersion wavelength of the fiber is estimated to be 1.1 $\mu$m) so continuum generation is mainly due to self-phase modulation, minimizing the noisy nonlinear processes that cause amplitude fluctuations. The self-phase
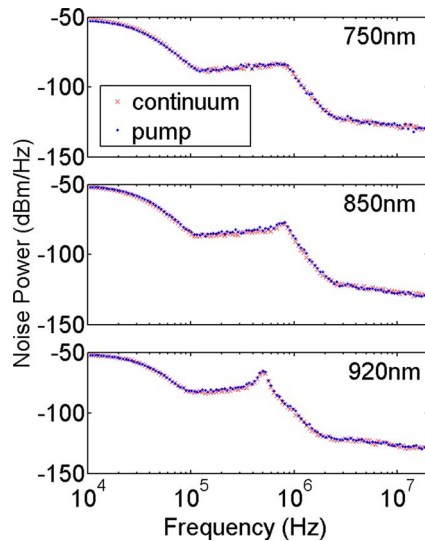
**Fig. 4** Noise spectra of the Ti-sapphire pump laser (blue) and the spectrally broadened beam (red) at 750, 850, and 920 nm center wavelength. There is less than 1.1 dBm/Hz difference between the pump and the broadened beam over the frequency range of 1 Hz to 25 MHz. (Color online only.)



**Fig. 5** Multiphoton and optical coherence microscopy images acquired at three different center wavelengths. The first, second, and third column corresponds to 750, 850, and 920 nm center wavelengths, respectively. (a–c) MPM images. (d–f) OCM images. (g–i) MPM images overlaid on OCM images to show spatial correspondence. (Color online only.)

modulation-dominated continuum generation is justified by the symmetric spectral broadening around the central wavelength of the pump (Fig. 3). The small asymmetric broadening at 920 nm pumping could be due to the decreased responsivity of the silicon detector in the spectrometer at the longest wavelengths. To verify stability, noise spectra were acquired of the pump and the supercontinuum beams at the three operating wavelengths using a fast diode and a radio frequency spectrum analyzer (Fig. 4). At these three wavelengths, there was less than 1.1 dBm/Hz difference in the noise over the frequency range of 1 Hz–25 MHz.

## 3 Imaging Results

### 3.1 OCM and MPM Imaging Across a Wide Spectral Range

OCM and MPM images were taken of green fluorescent protein (GFP)-transfected mouse fibroblast cells costained with two additional fluorescent markers. The GFP in this cell line is transfected to be coexpressed with vinculin, a cell-surface adhesion protein. The expression of GFP, therefore, can be correlated with the functional activity of these cells, such as cell–cell or cell–matrix interactions.[18] Although vinculin is found in the focal adhesion sites of cells, the GFP and vinculin are not believed to be bound together. Therefore, the fluorescence signal from GFP is expected to be distributed throughout the cytoplasm of the cells. Rhodamine B and $4',6$-diamidino-2-phenylindole (DAPI) were used to target the mitochondria and nucleus, respectively. OCM/MPM images were taken at different wavelengths throughout the tuning range of this source, corresponding to wavelengths where efficient two-photon absorption occurs for each fluorophore.[18] Bandpass optical filters were used to detect fluorescence from GFP (FF01-520/35, Semrock), DAPI (FF02-447/60, Semrock), and Rhodamine B (BG39, CVI Laser) since there is some overlap in the excitation spectra of these fluorophores
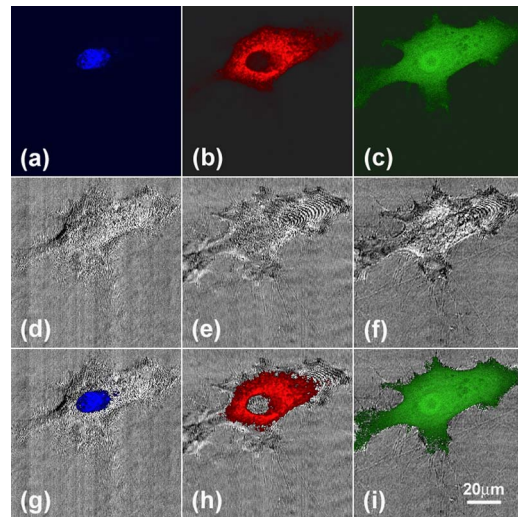
and also because Rhodamine B has a significantly higher two-photon cross section. At each wavelength, corresponding OCM images were acquired simultaneously.

The power of the broadband source was ~3 mW after the objective, while the narrowband source power varied between 5 and 10 mW, depending on the power needed for sufficient SNR in the MPM signal at each wavelength. Images were acquired in roughly 2 min using the scanning stage. The scanning range for the OCM and MPM images was $100 \times 100$ $\mu$m and images consist of $250 \times 250$ pixels. Pixel dwell time for MPM was 100 $\mu$s and OCM line scan rate was 10 kHz.

Figure 5 shows the MPM and the OCM images of a single cell separately, as well as the MPM images superimposed on the OCM images for registration and spatial correspondence. The three-dimensional position of the sample at each wavelength was unchanged. The MPM signal at 750, 850, and 920 nm targets the cell nucleus, the mitochondria, and the cytoplasm, respectively. The corresponding OCM images show the scattering structures of the whole cell. The simultaneous acquisition of OCM and MPM images allows the location of the functional fluorescent markers to be seen in the context of the structural environment of the whole sample. The OCM images show reflections from the culture dish, because this surface is highly scattering and the plane of imaging is within several micrometers of this interface. Differences in the OCM images can be attributed to both wavelength-dependent scattering and absorption in the sample, and to chromatic effects in the objective. Specifically, the image at 750 nm is focused at a point higher in the cell, while the image at 920 nm is focused lower and shows some details of the culture dish surface. This is due to the effects in the objective and can be compensated for by imaging at different planes depending on wavelength, or collecting three-dimensional volumes.

The dual-spectrum source allows each of the fluorescent markers to be efficiently excited at different wavelengths while maintaining the broad-bandwidth portion of the spectrum for OCM. The source extends the feasibility of performing OCM and MPM over a wider spectral range. Fluorescent dyes that are not efficiently excited using a broadband Ti-sapphire laser with a fixed center wavelength around 800 nm can be used with this source. A notably important fluorescent marker in cell biology, GFP, has an order-of-magnitude higher two-photon cross section in the range $920-1000$ nm compared to 800 nm.[19] The increased excitation efficiency enabled by tuning the wavelength also decreases adverse effects that can be caused by high-power, ultrafast lasers. To demonstrate the deep penetration depth of integrated OCM and MPM in highly scattering samples, images of human skin were taken *in vivo*.

### 3.2 OCM/MPM Imaging of Tissue

OCM and MPM images were simultaneously acquired from the dorsal surface of the hand of a human volunteer. Many proteins in the skin are autofluorescent and dyes are not typically needed to provide contrast in MPM. MPM excitation of skin at 770 nm induces an autofluorescence signal largely from NAD(P)H and flavines.[20] A low-pass emission filter (BG39, CVILaser, Livermore, CA) was used to detect the signal. The hand was stabilized using a custom-built mount with a thin glass window. MPM power incident on the skin was $<20$ mW and OCM power was $<5$ mW. In addition, the beam was blocked by a shutter when not being scanned. OCM and MPM images were acquired simultaneously in $\sim10$ s using galvanometer scanning. The pixel dwell time for MPM was $\sim150$ $\mu$s and line scan rate for OCM was 6.5 kHz. Images consisted of $250\times250$ pixels. Four images at each depth were averaged to improve the SNR of the MPM images and reduce speckle in the OCM images. Figure 6 shows OCM and MPM images from three layers of the skin: the stratum corneum, stratum spinosum, and the superficial dermis. Individual keratinocytes can be visualized in the MPM channel due to the autofluorescent proteins in the cytoplasm. OCM can also visualize the locations of cell nuclei based on forward-scattering, resulting in darker, low-backscattering regions where nuclei are located. The large round structures in the superficial dermis (Fig. 6(e) and 6(f)) that are visible in both the OCM and MPM channels are papillae, projections of the dermis into the epidermis. Although the OCM and MPM images visualize some of the same features in this unstained tissue, it is important to realize that these two imaging modalities are based on different contrast mechanisms. Potential applications include tracking functional dynamics in *in vivo* tissue, or tracking of single or small populations of labeled cells after injection or transplantation.

### 4 Conclusions

In summary, we have demonstrated a novel single-laser dual-spectrum source for integrated OCM/MPM imaging based on spectrally broadening a widely tunable Ti-sapphire laser by continuum generation in a photonic crystal fiber. The broadening of the spectrum is both sufficient for high-sensitivity OCM and stable over a large tuning range. With this source, a broader range of fluorescent markers can be optimally tar-
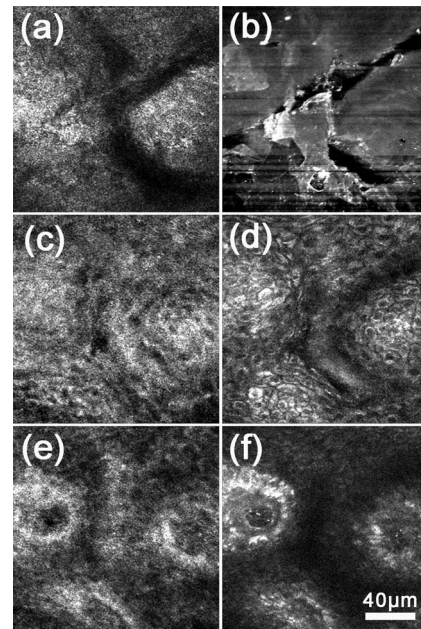


**Fig. 6** Simultaneously captured OCM (a, c, e) and MPM (b, d, f) images of *in vivo* human skin acquired from three different skin layers. The stratum corneum (a, b), the stratum spinosum (c, d), and the superficial dermis (e, f) can be visualized at cellular-level resolution with both imaging modalities. The MPM images show autofluorescence from NAD(P)H and flavines in the cells while the OCM images show the optical scattering from the cells and extracellular matrix.

geted while maintaining a broad bandwidth for OCM imaging. This increases the feasibility of this multimodality imaging approach for investigations in *in vivo* tissue or in various tissue models. Future work will investigate additional contrast enhancement through spectroscopic OCM analysis over the large wavelength range made possible by this source.

### References

1. J. A. Izatt, M. R. Hee, G. M. Owen, E. A. Swanson, and J. G. Fujimoto, "Optical coherence microscopy in scattering media," *Opt. Lett.* **19**, 590–592 (1994).
2. V. E. Centonze and J. G. White, "Multiphoton excitation provides optical sections from deeper within scattering specimens than confocal imaging," *Biophys. J.* **75**, 2015–2024 (1998).
3. A. T. Yeh, B. Kao, W. G. Jung, Z. Chen, J. S. Nelson, and B. J. Tromberg, "Imaging wound healing using optical coherence tomography and multiphoton microscopy in an *in vitro* skin-equivalent tissue model," *J. Biomed. Opt.* **9**, 248–253 (2004).
4. S. Yazdanfar, Y. Y. Chen, P. T. C. So, and L. H. Laiho, "Multifunctional imaging of endogenous contrast by simultaneous nonlinear and optical coherence microscopy of thick tissues," *Microsc. Res. Tech.* **70**, 628–633 (2007).
5. S. Tang, C. Sun, T. B. Krasieva, Z. Chen, and B. J. Tromberg, "Im-

aging subcellular scattering contrast by using combined optical coherence and multiphoton microscopy," *Opt. Lett.* **32**, 503–505 (2007).

6. S. Tang, T. B. Krasieva, Z. Chen, G. Tempea, and B. J. Tromberg, "Effect of pulse duration on two-photon excited fluorescence and second harmonic generation in nonlinear optical microscopy," *J. Biomed. Opt.* **22**, 020501 (2006).

7. U. Morgner, W. Drexler, F. X. Kartner, X. D. Li, C. Pitris, E. P. Ippen, and J. G. Fujimoto, "Spectroscopic optical coherence tomography," *Opt. Lett.* **25**, 111–113 (2000).

8. C. Xu, C. Vinegoni, T. S. Ralston, W. Luo, W. Tan, and S. A. Boppart, "Spectroscopic spectral-domain optical coherence microscopy," *Opt. Lett.* **31**, 1079–1081 (2006).

9. E. Beaurepaire, L. Moreaux, F. Amblard, and J. Mertz, "Combined scanning optical coherence and two-photon excited fluorescence microscopy," *Opt. Lett.* **24**, 969–971 (1999).

10. C. Vinegoni, T. Ralston, W. Tan, W. Luo, D. L. Marks, and S. A. Boppart, "Integrated structural and functional optical imaging combining spectral-domain optical coherence and multiphoton microscopy," *Appl. Phys. Lett.* **88**, 053901 (2006).

11. S. Tang, T. B. Krasieva, Z. Chen, and B. J. Tromberg, "Combined multiphoton microscopy and optical coherence tomography using a 12-fs broadband source," *J. Biomed. Opt.* **11**, 020502 (2006).

12. C. Joo, K. Kim, and J. de Boer, "Spectral-domain optical coherence phase and multiphoton microscopy," *Opt. Lett.* **32**, 623–625 (2007).

13. T. M. Lee, A. L. Oldenburg, S. Sitafalwalla, D. L. Marks, W. Luo, F. J. Toublan, K. S. Suslick, and S. A. Boppart, "Engineered microsphere contrast agents for optical coherence tomography," *Opt. Lett.*

14. D. L. Marks, A. L. Oldenburg, J. J. Reynolds, and S. A. Boppart, "Study of an ultrahigh-numerical-aperture fiber continuum generation source for optical coherence tomography," *Opt. Lett.* **27**, 2010–2012 (2002).

15. J. K. Ranka, R. S. Windeler, and A. J. Stentz, "Visible continuum generation in air-silica microstructure optical fibers with anomalous dispersion at 800 nm," *Opt. Lett.* **25**, 25–27 (2000).

16. G. Humbert, W. Wadsworth, S. Leon-Saval, J. Knight, T. Birks, P. St. J. Russell, M. Lederer, D. Kopf, K. Wiesauer, E. Breuer, and D. Stifter, "Supercontinuum generation system for optical coherence tomography based on tapered photonic crystal fibre," *Opt. Express* **14**, 1596–1603 (2006).

17. H. Tu, D. L. Marks, Y. L. Koh, and S. A. Boppart, "Stabilization of continuum generation from normally dispersive nonlinear optical fibers for a tunable broad bandwidth source for optical coherence tomography," *Opt. Lett.* **32**, 2037–2039 (2007).

18. W. Tan, C. Vinegoni, J. J. Norman, T. A. Desai, and S. A. Boppart, "Imaging cellular responses to mechanical stimuli within three-dimensional tissue constructs," *Microsc. Res. Tech.* **70**, 361–371 (2007).

19. C. Xu, W. Zipfel, J. B. Shear, R. M. Williams, and W. W. Webb, "Multiphoton fluorescence excitation: New spectral windows for biological nonlinear microscopy," *Proc. Natl. Acad. Sci. U.S.A.* **93**, 10763–10768 (1996).

20. K. Konig and I. Riemann, "High-resolution multiphoton tomography of human skin with subcellular spatial resolution and picosecond time resolution," *J. Biomed. Opt.* **8**, 432–439 (2003).

**28**, 1546–1548 (2003).